HHS Public Access

Author manuscript

Oncogene. Author manuscript; available in PMC 2011 February 16.

Published in final edited form as:

Oncogene. 2010 July 22; 29(29): 4170–4182. doi:10.1038/onc.2010.170.

EVIDENCE FOR MESENCHYMAL-LIKE SUBPOPULATIONS WITHIN SQUAMOUS CELL CARCINOMAS POSSESSING CHEMORESISTANCE AND PHENOTYPIC PLASTICITY

Devraj Basu, MD, PhD[1,2,3], **Thierry-Thien K. Nguyen, MS**[3], **Kathleen T. Montone, MD**[4], **Gao Zhang, BS**[3], **Li-Ping Wang, BS**[4], **J. Alan Diehl, PhD**[5], **Anil K. Rustgi, MD**[6], **John T. Lee, PhD**[3], **Gregory S. Weinstein, MD**[1], and **Meenhard Herlyn, DVM, DSc**[3]

[1] Department of Otorhinolaryngology-Head and Neck Surgery, University of Pennsylvania, Philadelphia, Pennsylvania

[2] Veterans Administration Medical Center, Philadelphia, Pennsylvania

[3] The Wistar Institute, Philadelphia, Pennsylvania

[4] Department of Pathology and Laboratory Medicine, University of Pennsylvania, Philadelphia, Pennsylvania

[5] Department of Cancer Biology, University of Pennsylvania, Philadelphia, Pennsylvania

[6] Department of Medicine, University of Pennsylvania, Philadelphia, Pennsylvania

Abstract

Variable drug responses among malignant cells within individual tumors may represent a barrier to their eradication using chemotherapy. Carcinoma cells expressing mesenchymal markers resist conventional and epidermal growth factor receptor (EGFR)-targeted chemotherapy. Here we evaluated whether mesenchymal-like subpopulations within human squamous cell carcinomas (SCCs) with predominantly epithelial features contribute to overall therapy resistance. We identified a mesenchymal-like subset expressing low E-cadherin (Ecad-lo) and high vimentin (Vim-hi) within upper aerodigestive tract SCCs. This subset was both isolated from cell lines and identified in xenografts and primary clinical specimens. The Ecad-lo subset contained more low-turnover cells, correlating with resistance to the conventional chemotherapeutic paclitaxel *in vitro*. Epidermal growth factor (EGF) induced less stimulation of the MAP kinase and PI3-kinase pathways in Ecad-lo cells, which was likely due to lower EGFR expression in this subset and correlated with *in vivo* resistance to the EGFR-targeted antibody cetuximab. The Ecad-lo and high E-cadherin (Ecad-hi) subsets were dynamic in phenotype, showing the capacity to repopulate each other from single cell clones. Taken together, these results provide evidence for a low-turnover,

Corresponding authors: Meenhard Heryln and Devraj Basu, The Wistar Institute, 3601 Spruce St., Philadelphia, PA, 19104. Phone: 215 898-3950; Fax: 215 898-0980; herlynm@wistar.org, devraj.basu@uphs.upenn.edu.

Conflict of Interest

All authors declare no conflict of interest.

mesenchymal-like subpopulation in SCCs with diminished EGFR pathway function and intrinsic resistance to conventional and EGFR-targeted chemotherapies.

Keywords

EMT; squamous cell carcinoma; head and neck; chemotherapy resistance; tumor heterogeneity

INTRODUCTION

The inability to eradicate SCCs of the upper aerodigestive tract, including those of the head and neck (HNSCC) and esophagus (ESCC), with chemotherapy alone is a feature shared with most other malignancies. Drug therapy for advanced stage HNSCC has benefited from two recent advances: inclusion of paclitaxel in conventional chemotherapy regimens (Posner *et al.*, 2007; Vermorken *et al.*, 2007) and introduction of the EGFR-targeted antibody cetuximab into clinical use (Bonner *et al.*, 2006; Herbst *et al.*, 2005). Although these agents can produce dramatic responses, cancer recurrence is inevitable without addition of other therapeutic modalities, and treatment failures are common even with use of combined modalities. Thus, identifying and targeting minority SCC subpopulations with intrinsic resistance to these two agents is an appealing strategy for tumor eradication.

Epithelial to mesenchymal transition (EMT) generates phenotypic heterogeneity within SCCs and is one potential basis for defining subpopulations with intrinsic drug resistance. The hallmark of EMT is loss of cell surface E-cadherin, which accompanies disassembly of adherens junctions, acquired motility, and expression of mesenchymal markers including vimentin, N-cadherin, and fibronectin (Christiansen and Rajasekaran, 2006; Hugo *et al.*, 2007). The EMT program is coordinated by multiple transcription factors, including the Twist, Snail, and Zeb families (Ansieau *et al.*, 2008; Cano *et al.*, 2000; Peinado *et al.*, 2007). Originally characterized as an embryologic process that drives cell migration and diversifies phenotype, EMT concepts remain controversial in application to cancer biology. While recognizable in carcinoma lines, the dramatic phenotypic shifts of EMT are generally not observed to similar extent *in vivo* (Tarin *et al.*, 2005), and it is doubtful whether carcinomas ever fully acquire mesenchymal features to parallel events during development. However, a range of mesenchymal traits do exist across SCCs, and we therefore favor the label “mesenchymal-like” to designate phenotypes arising from EMT in malignancy.

Thus far, drug resistance arising from EMT has been assessed mainly by comparing cell lines possessing or lacking prominent expression of mesenchymal markers, based on the premise that this property distinguishes two subtypes of tumors. Several studies have correlated mesenchymal-like traits with higher overall resistance to conventional cytotoxic chemotherapies (Wang *et al.*, 2009; Yang *et al.*, 2006) and EGFR inhibitors (Fuchs *et al.*, 2008; Thomson *et al.*, 2005; Yauch *et al.*, 2005). However, carcinomas rarely fall cleanly into dichotomous epithelial or mesenchymal-like categories *in vivo* and instead show either predominantly epithelial features or a spectrum of mixed epithelial and mesenchymal-like differentiation (Strauss *et al.*, 2009). It is presently unclear whether the intrinsic drug resistance in “mesenchymal” carcinoma lines is actually attributable to discrete

mesenchymal-like subpopulations within them and whether comparable populations *in vivo* play a similar role.

Here we identify and isolate a minority mesenchymal-like subpopulation from SCCs bearing predominantly epithelial features. Distinctive growth and EGFR-signaling properties are identified in this subset and correlated with intrinsic resistance to paclitaxel and cetuximab *in vitro*. In addition, cetuximab resistance of these cells is evaluated *in vivo* using direct xenografts of human primary tumors. To clarify the developmental relationship between the epithelial and mesenchymal-like subpopulations, the phenotypic stability of each is tracked at a clonal level.

RESULTS

SCCs contain distinct epithelial and mesenchymal-like subpopulations *in vitro* and *in vivo*

Initially, the variability in epithelial versus mesenchymal-like differentiation was defined in a panel of ten SCC cell lines, which segregated into three general patterns based on E-cadherin and vimentin staining. One end of the spectrum is represented by the SCC15, TE12, and SCC13 cell lines, which demonstrate diffuse E-cadherin expression and limited or no vimentin-staining (Figure S1A). TE1, SCC9, OCTT2, and TE9 cells represented and intermediate pattern, with distinct E-cadherin and vimentin-positive populations, and, in the case of TE9, a sizeable subset expressing both markers (Figure S1B). The other extreme is exemplified by the SCC4, TE8, and HCE4 cell lines, which show diffuse vimentin staining and minimal E-cadherin-expressing cells (Figure S1C).

To facilitate a study of mesenchymal-like subsets in tumors with predominantly epithelial features, we selected two HNSCC lines (SCC9 and OCTT2) containing minority subpopulations sizeable enough to isolate. These lines appeared heterogeneous in culture, with clustered epithelial-like cells interspersed with fusiform mesenchymal-like morphologies (Figure 1A, left panels). Both lines were comprised mostly of non-overlapping Ecad-hi/Vim-lo and Ecad-lo/Vim-hi populations (Figure 1A, right panels). The minimal overlap between these phenotypes was confirmed by segregating each line into Ecad-hi and Ecad-lo groups (Figure 1B, top) by fluorescence-activated cell sorting (FACS) and demonstrating vimentin staining reciprocal to E-cadherin expression in sorted subsets (Figure 1B, bottom). To confirm that Ecad-lo cells possess mesenchymal-like differentiation, gene expression profiles of Ecad-hi and Ecad-lo populations were compared. SCC9 and OCTT2 Ecad-lo cells up-regulated multiple genes associated with EMT (Figure 1C, left) and also down-regulated genes characteristic of epithelial phenotypes (Figure 1C, right). These findings confirmed that FACS-purification of Ecad-hi and Ecad-lo cells was a valid method of segregating the epithelial and mesenchymal-like subsets. Thus the terms “Ecad-hi” and “Ecad-lo” are subsequently used interchangeably with “epithelial” and “mesenchymal-like” in reference to SCC9 and OCTT2 cells.

Mesenchymal-like subpopulations were identified *in vivo* using dual immunohistochemistry (IHC) staining for E-cadherin and vimentin. Mouse xenografts of the SCC9 line contained a small vimentin positive subset with fusiform morphology, distinct from the E-cadherin-positive majority (Figure 1D, top left). To enhance the visual contrast between vimentin and

E-cadherin staining, chromogens were digitally converted to red and green pseudo-colors, respectively (Figure 1D, bottom left). A vimentin-expressing subpopulation was also observed in the original human primary tumor from which the OCTT2 line was derived (Figure 1D, middle), although detection of nonmalignant stromal cells by the human-specific vimentin antibody could not be excluded here. For this reason, a similar vimentin-positive subset was sought and identified in a direct xenograft of this primary tumor (Figure 1D, right). Here mouse passage is expected to deplete all nonmalignant human cells, and use of human-specific antibody prevented labeling of mouse-derived stromal cells within xenografts. The malignant potential of the mesenchymal-like subset was demonstrated by comparing *in vivo* growth of sorted Ecad-hi versus Ecad-lo cells from the OCTT2 cell line (Figure S2). As xenografts, these purified subsets showed no major differences in latency, growth, histology, or distribution of mesenchymal-like cells in mature tumors. The broad *in vivo* relevance of the vimentin-positive subpopulation is underscored by SCC9 and OCTT2 tumors representing opposites in the spectrum of HNSCC grades, from well-differentiated to poorly differentiated (Figure S3).

The mesenchymal-like subset contains more low-turnover cells

To determine whether the mesenchymal-like subpopulation had altered growth features, proliferation of Ecad-hi and Ecad-lo SCC9 cells was compared by MTT assay, which demonstrated slower growth in the Ecad-lo compartment (Figure 2A). Reduced growth of Ecad-lo cells coincided with a higher proportion in G0/G1 phase by cell cycle analysis (Figure 2B) and double the percentage in resting G0 phase, as defined by absence of Ki-67 expression (Figure 2C). The turnover characteristics of Ecad-hi and Ecad-lo subpopulations were compared over an extended period, based on dilution of the fluorescent membrane label PKH-67 with ongoing cell division. After uniform PKH-67 labeling, SCC9 cells were grown in culture for 9 days to create a broad distribution of PKH-67 intensity (Figure 2D). Low and high turnover subsets were defined as populations with the 10% highest and 10% lowest PKH-67 label, respectively. Low turnover (high label-retaining) SCC9 cells contained over 5-fold more Ecad-lo cells relative to high turnover (low label-retaining) cells. Taken together, these results indicated that the mesenchymal-like subpopulation contains a larger proportion of low turnover cells and is less proliferative overall.

The mesenchymal-like subpopulation shows intrinsic resistance to paclitaxel

To assess whether diminished growth of the mesenchymal-like subset correlates with paclitaxel resistance, FACS segregated Ecad-hi and Ecad-lo cells were compared for drug-induced growth inhibition (Figure 3A). The half-maximal growth inhibitory concentration (IC50) for Ecad-lo cells was 2-log higher in SCC9 and 1.5-log higher in OCTT2, relative to Ecad-hi cells, using a 4 hour drug exposure. Prolonging the drug exposure time to 48 hours minimally impacted this difference in IC50 for OCTT2 and diminished it to a still-significant 0.75 log for SCC9 (Figure S4). Unsorted SCC9 cells also showed evidence of paclitaxel resistance in the Ecad-lo subset, which became enriched from 18% to 50% in cultures after brief drug exposure (Figure 3B, left and second panel). To exclude that paclitaxel down-regulated E-cadherin without truly enlarging the mesenchymal-like subpopulation, Ecad-lo and Ecad-hi cells surviving treatment were demonstrated to retain Vim-hi and Vim-lo phenotypes, respectively. (Figure 3B, third panel). Despite a decrease in

IC50 for SCC9 Ecad-lo cells with prolonged drug exposure, 48 hours of treatment did not reduce the enrichment of Ecad-lo cells (Figure 3B, right panel). Growth potential of Ecad-hi and Ecad-lo cells surviving paclitaxel was defined by comparing their clonogenicity (Figure 3C, left) and proliferation (right). While treating Ecad-hi cells reduced their clonogenicity and overall growth, paclitaxel minimally impacted these properties in surviving Ecad-lo cells. These results demonstrated that the Ecad-lo subset not only possessed elevated intrinsic resistance to killing by paclitaxel but also maintained growth potential post-therapy.

SCC9 cultures were tracked by video to distinguish whether paclitaxel enriched the Ecad-lo subset by selectively depleting Ecad-hi cells or by causing differentiation toward the mesenchymal-like phenotype. Videos of untreated cells contrast rapidly dividing cells of epithelial morphology against slowly proliferative but more migratory cells of mesenchymal appearance (Video 1). In treated cells, cell death localized to areas with epithelial morphology, sparing regions with mesenchymal-like differentiation (Video 2 and Figure 3D). This finding demonstrated that the Ecad-hi subset was selectively killed by paclitaxel and suggested its depletion as the major mechanism behind relative expansion of the Ecad-lo subpopulation.

Decreased EGFR expression in the mesenchymal-like subset correlates with diminished regulation of MAPK/PI3K pathways by EGFR ligand

The EGFR-targeted antibody cetuximab is another key agent in clinical use against SCCs. To assess potential responsiveness of the mesenchymal-like subpopulation to EGFR targeting, we compared the integrity of EGFR signaling pathways between the Ecad-lo and Ecad-hi subsets. Flow cytometry (FC) of SCC9 and OCTT2 lines identified decreased surface EGFR expression in the Ecad-lo versus Ecad-hi subsets (Figure 4A, left/middle). Reduced surface EGFR expression in the Ecad-lo subset was also demonstrated *in vivo* by analyzing disaggregated xenografts of the tumor from which the OCTT2 line was derived (Figure 4A, right). This reduction in surface EGFR corresponded with diminished total EGFR levels in the mesenchymal like subset, as shown by immunofluorescence (IF) staining (Figure S5A), FC of permeabilized cells (Figure S5B), and western blot (Figure S5C).

We assessed whether EGFR down-regulation in Ecad-lo cells corresponded with diminished capacity of the receptor to regulate the downstream phosphatidylinositol-3-kinase (PI3K) and mitogen-activated protein kinase (MAPK) pathways. Minimal activation of both ERK (Figure 4B) and AKT (Figure 4C) was seen in serum-starved vimentin-positive SCC9 cells upon addition of EGF, in contrast to prominent activation of both molecules by ligand in vimentin-negative cells. Costaining for E-cadherin in place of vimentin confirmed a pattern of selective ERK/AKT activation in the Ecad-hi subset by EGFR ligand (Figure S6). Taken together, these results provide evidence that the MAPK and PI3K pathways are uncoupled from regulation by EGFR-specific ligands in Ecad-lo cells, most likely as a consequence of decreased EGFR expression in this subset.

The mesenchymal-like subpopulation shows intrinsic resistance to cetuximab *in vitro* and *in vivo*

Reduced signaling through EGFR in the Ecad-lo subset predicted diminished responsiveness to cetuximab. Accordingly, cetuximab showed greater activity against Ecad-hi cells in both SCC9 and OCTT2 (Figure 5A). To assess whether the mesenchymal-like subset was cetuximab-resistant *in vivo*, mice xenografted with the tumor of origin for the OCTT2 cell line were treated with cetuximab. Partial regression of established tumors was observed over 12 days, during which time saline-treated controls grew rapidly (Figure 5B). Dual label IHC staining of treated tumors showed a marked increase in vimentin-expressing areas relative to controls (Figure 5C, first row), and visual contrast between the dual subpopulations was enhanced by pseudo-coloring the chromogens (second row). Dual IHC-stained tumors were analyzed to quantify the increase in vimentin staining area by comparing wide fields of treated and untreated tumors (third row). Calculating relative sizes of vim-hi versus vim-lo areas (mapped in red and green, fourth row) revealed a greater than 2-fold increase in vim-hi regions with cetuximab treatment (Figure 5D). These results strongly suggest that selective targeting of the Ecad-hi subpopulation via cetuximab enriched the mesenchymal-like subset, either through depletion of epithelial cells and/or increasing their differentiation toward a mesenchymal-like phenotype.

Epithelial and mesenchymal-like phenotypes are reversible at a clonal level

The observed therapy resistance of the Ecad-lo cells warranted investigation of their capacity to repopulate Ecad-hi components of tumors. To clarify developmental relationships between these two subpopulations, the phenotypic stability of each was tracked using clones of single SCC9 cells. Morphologically homogeneous colonies arising from single Ecad-hi or Ecad-lo cells were confirmed for purity based on exclusive E-cadherin or vimentin staining, and similar colonies were expanded and tracked for development of heterogeneity. Epithelial colonies arising from Ecad-hi cells rapidly reconstituted a mesenchymal-like subset, detectable within two weeks of plating at clonal density (Figure 6A). Mesenchymal-like colonies from Ecad-lo cells showed phenotypic stability upon initial expansion. However, these colonies reconstituted the epithelial subset on further growth, with early evidence of a small Ecad-hi subpopulation appearing at 4 weeks and expansion of this subset noted by 8 weeks (Figure 6B). These results indicated that the mesenchymal-like subpopulation is not terminally differentiated and suggested that it retains the plasticity to reconstitute other malignant subsets post-therapy.

DISCUSSION

In this study we demonstrate that mesenchymal-like malignant subpopulations contribute to chemotherapy resistance in SCCs with predominantly epithelial differentiation. Previous studies correlated drug resistance in carcinoma lines with increased expression of mesenchymal markers (Frederick *et al.*, 2007; Ghoul *et al.*, 2009; Shrader *et al.*, 2007; Thomson *et al.*, 2005; Yang *et al.*, 2006; Yauch *et al.*, 2005). However, analyzing lines as total populations does not account for the possible presence of epithelial and mesenchymal-like subsets, which may make disparate contributions to overall drug resistance. We suggest that SCCs *in vivo* typically do not possess uniformly epithelial or mesenchymal-like

phenotypes; accordingly, the heterogeneity defined here in SCC cell lines was maintained by their *in vivo* counterparts. Consistent with this observation, a study examining several HNSCC histologic types revealed heterogeneous vimentin staining to be typical, with only a rare subtype, the “sarcomatoid” carcinoma, expressing uniformly high levels throughout (Mandal *et al.*, 2008). At the other end of the spectrum, cell lines with high E-cadherin expression can still contain small vimentin-expressing subsets (Figure S1), and we note the same observation in xenografts of human HNSCC specimens (unpublished data). Nevertheless, it is unlikely that the precise markers used here to define the treatment resistant subpopulation will identify subsets with similar properties across all SCCs. We speculate that more subtle phenotypic transitions sharing key molecular traits with the ones documented here may be a basis for intrinsic treatment resistance across many SCC tumors.

In this study, intrinsic paclitaxel resistance of the mesenchymal-like subpopulation seemed attributable to its slower growth. However, cytotoxic drug resistance after EMT is likely more than a direct function of growth rate and instead reflects the outcome of gene-regulatory programs with complex relationships to proliferation, differentiation, and apoptosis. For instance, a recent study showed that paclitaxel induces snail and slug, which, in addition to being transcription factor mediators of EMT, also repressed promoters of key molecules involved in p53-mediated apoptosis (Kurrey *et al.*, 2009). Thus, at least *in vitro*, paclitaxel likely depletes the epithelial subset by multiple mechanisms and may also contribute to enrichment of mesenchymal-like cells by promoting EMT. Similarly, adriamycin, a cytotoxic drug of differing mechanism, also enhances EMT and creates resistance to itself and other agents as a twist1-mediated phenomenon (Li *et al.*, 2009b).

Resistance to cetuximab in the Ecad-lo subset here likely arose from reduced EGFR expression and resulting loss of MAPK and PI3K pathway regulation by the receptor. This correlation contrasts with the lack of positive association between EGFR over-expression and clinical cetuximab sensitivity in HNSCC (Kalyankrishna and Grandis, 2006). Our findings also differ with a study of hepatocellular carcinoma cell lines, where EGFR levels appeared independent of mesenchymal marker expression (Fuchs *et al.*, 2008). However, EGFR expression had thus far been compared against mesenchymal features using bulk lines, where overall receptor levels may not reflect those of any mesenchymal-like subsets they contain.

Known resistance mechanisms to EGFR-targeted therapies (Bianco *et al.*, 2005; Cooper and Cohen, 2009) provide context for understanding the cetuximab insensitivity observed here. A novel mechanism for acquired cetuximab resistance is ligand-independent EGFR function through down-regulation of surface receptor and elevated nuclear, cytoplasmic, and total receptor levels (Li *et al.*, 2009a). This mechanism may partly explain the association in HNSCCs of EGFR gene amplification and poor prognosis (Chung *et al.*, 2006; Temam *et al.*, 2007), but the reduced surface and total EGFR here in Ecad-lo cells argues against this explanation for their resistance. An alternative explanation is switching to other receptor tyrosine kinases to restore downstream survival and proliferation signals. For instance, EGFR and ErbB2 expression were noted to segregate to different regions within ESCCs (Kawaguchi *et al.*, 2007) and thus might serve comparable functions in distinct subpopulations. Also, EGFR down-regulation and coordinate up-regulation of ErbB2/ErbB3

in HNSCC are described in response to the EGFR-targeted small molecule gefitinib (Erjala *et al.*, 2006). Kinase switching to receptors outside the EGFR family is observed in mesenchymal-like cell lines of non small cell lung cancers (NSLC) (Thomson *et al.*, 2005) and is a plausible mechanism here. Notably, the EGFR activating mutations that sensitize NSLC to gefitinib (Gazdar, 2009) are largely absent in HNSCC (Temam *et al.*, 2007), and thus sensitivity to this inhibitor is not anticipated in the face of cetuximab resistance.

Traits of the mesenchymal-like subpopulation in SCCs have implications in the wider discussion regarding origins of phenotypic heterogeneity within solid tumors. Specifically, it remains unclear how much intra-tumor heterogeneity arises from epigenetic differences versus genetic change driven by clonal evolution (Shackleton *et al.*, 2009). The ability of epithelial and mesenchymal-like subsets to reconstitute each other from single cell clones, as shown here, suggests that these phenotypes are distinguished primarily by epigenetic alterations and not genotypic selection. The cancer stem cell hypothesis is one framework for explaining how an epigenetically distinct subpopulation may sustain tumor growth and resist drug therapy. We have elected here not to frame the mesenchymal-like subset explicitly within controversial and evolving definitions of cancer stem cells; however, this subset appears to maintain malignant potential and does not represent a terminally differentiated phenotype. The subpopulation in SCC may have functions analogous to the CD44+/CD24− stem-like subset in breast carcinoma on the basis of sharing its mesenchymal-like gene expression profile (Mani *et al.*, 2008). If so, the *in vitro* plasticity of our subpopulations argues against a rigid developmental hierarchy originating with stem cells and ending in terminal differentiation, instead favoring one where phenotypes are dynamic and sensitive to microenvironments. It is possible that the mesenchymal-like subset in SCCs retains the phenotypic plasticity to repopulate other subpopulations post therapy.

In context of our findings, promoting phenotypic reversal of Ecad-lo cells through mesenchymal to epithelial transition (MET) may be a viable strategy for chemosensitization. Here pure mesenchymal-like clones of SCC lines showed initial resistance to MET but did restore the epithelial subpopulation spontaneously after extended culture. Experimental maneuvers that both promote MET and enhance drug sensitivity include down-regulation of Notch (Wang *et al.*, 2009), induction of Raf-kinase inhibitor protein (Wu and Bonavida, 2009), knockdown of zeb-1 (Haddad *et al.*, 2009), and induction of miR-200 microRNA family members (Adam *et al.*, 2009; Gregory *et al.*, 2008; Li *et al.*, 2009c). Future studies will seek pharmacologic strategies for both specifically targeting the mesenchymal-like subpopulation in SCCs and promoting its phenotypic reversal.

MATERIALS AND METHODS

Cell lines and clinical specimens

Cell lines were maintained in 1:1 Dulbecco's modified Eagle and Ham's F12 media, with 400ng/ml hydrocortisone and 10% fetal calf serum. Genetic purity of cell lines was confirmed with an Identify Mapping Kit (Coriell Institute, Camden, NJ, USA). SCC9, SCC4, and SCC15 cells were obtained from the ATCC (CRL-1629, 1624, 1623). TE12, SCC13, TE1, TE9, TE8, and HCE4 cell lines are previously described (Okano *et al.*, 2000; Opitz *et al.*, 1998). The OCTT2 cell line was derived from a surgical specimen of an oral

HNSCC in compliance with University of Pennsylvania Institutional Review Board-approved protocol #417200. Tumor cells purified from xenografts of this specimen were seeded at 5000 cells/cm^2 on mitomycin C-treated 3T3 fibroblasts and cultured as described (Rheinwald and Beckett, 1981).

Animals and *in vivo* experiments

Non-obese diabetic/severe combined immunodeficient/interleukin-2 receptor γ-chain-deficient mice were used in all experiments. Animals were bred and utilized at the Wistar Institute animal facility under protocols approved by the institutional animal care and use committee. To generate xenografts from human SCC specimens, 1mm tumor fragments were placed in subcutaneous pockets through flank incisions in anesthetized mice. Growth Factor Reduced Matrigel (BD, Franklin Lakes, NJ, USA) was added, and incisions were closed with suture. Xenografts were utilized prior to 10 *in vivo* passages, and tumor volumes were measured as [length × width × thickness]. Xenografts of SCC9 cells were generated by subcutaneous injection of 2×10^6 cells in 100μl Matrigel. For drug treatment, 1mg cetuximab (Imclone, New York, NY, USA) or equivalent volume saline control was injected intraperitoneally every three days.

Microscopy

Images obtained using Nikon TE2000 and E600 microscopes were processed with ImagePro-Plusv6.2 and ACT-1 software using uniform settings within each experiment. For video microscopy, SCC9 cells cultured in 6-well plates were treated with paclitaxel or control dimethylsulfoxide (DMSO). Drug was removed after 4 hours, and medium was supplemented with 20 μg/ml propidium iodide (PI). Cell death (PI uptake) was monitored using a Nikon TE300 microscope configured with automated filter wheels and stage, and an environmental chamber. Three fields/well were captured at 10-minute intervals and sequenced into video using ImagePro-Plus.

Immunofluorescence staining

IF staining was performed in 24-well plates or gelatin-coated glass chamber slides, as described (Smalley *et al.*, 2005). Antibodies of the following specificities were used: Alexafluor488-E-cadherin (BD), phosphoERK1/2-Thr202/Tyr204 (pERK), phosphoAKT-Ser473 (pAKT) (Cell Signaling, Danvers, MA, USA), vimentin (AnaSpec, Fremont, CA, USA), vimentin (Dako, Carpinteria, CA). Secondary antibodies included alexafluor488-anti-rabbit IgG, alexafluor594-anti-human IgG, and alexafluor594-anti-rabbit IgG (Invitrogen, Carlsbad, CA, USA). Isotype-matched mouse and rabbit antibodies were used as controls. In signaling experiments, cells were serum-starved for 24 hours before treatment with 200ng/ml recombinant human EGF (Invitrogen) for 1 hour.

Flow cytometry, cell sorting, tumor cell purification from xenografts

A FACSAria (BD) sorter was used for FACS. FC was performed using a FACSCalibur instrument (BD) and analyzed using WinMDIv2.9. Dead cells were removed by exclusion of either PI or 7-amino-actinomycin-D positive cells. Where required for intracellular staining, sorted cells were permeabilized with acetone, as described (Mancaniello and

Carbonari, 2008). Cell cycle analysis was performed as previously described (Smalley *et al.*, 2006). FC staining (Fang *et al.*, 2005) was performed with the following human specific antibodies: fluorescein isothiocyanate (FITC)-Ki-67, allophycocyanin (APC)-E-cadherin (Biolegend, San Diego, CA, USA), phycoerythrin (PE)-vimentin (Abcam, Cambridge, MA, USA), FITC-EGFR (Santa Cruz Biotech., Santa Cruz, CA, USA), FITC mouse $IgG_{1,\kappa}$ control (BD), APC mouse IgG_1 control, and PE mouse IgG_1 control (BD). PKH-67 labeling was performed per supplier protocol (Sigma, St. Louis, MO, USA).

To FACS-purify tumor cells from xenografts, minced tumors were digested overnight at 4°C in culture medium containing 2mg/ml collagenase-I and 1mg/ml collagenase-IV. Suspensions were passed through 40μm filters and pretreated with rat anti-mouse CD16/32 (Fc-Block, BD). Mouse-derived cells were excluded by positive selection of human cells with mouse anti-human major histocompatibility class I (Abcam) and PE-anti-mouse IgG $F(ab)_2$ secondary antibody (Sigma).

Dual label immunohistochemistry, processing of images

Formalin-fixed, paraffin-embedded specimens were cut in 5μm sections, and antigens were retrieved by boiling for 15 minutes in EDTA buffer (Lab Vision, Fremont, CA, USA). Staining was performed sequentially for E-cadherin and vimentin, using the Envision Detection Kit (Dako), followed by hematoxylin counterstain. Mouse anti-human E-cadherin (Dako) was used at 1:10 dilution and detected with 3′,3-diaminobenzidine (DAB). After re-quenching peroxidase activity, mouse anti-human vimentin (Dako) was used without dilution and detected using Vector VIP (V-VIP) chromogen (Vector, Burlingame, CA, USA). Specificity was confirmed using mouse IgG1 controls for each antibody. To generate pseudo-colored images, IHC micrographs were processed using Adobe Photoshop CS2. Color ranges corresponding to DAB and V-VIP-stained areas were separated using histogram analysis and color-replaced with green and red, respectively. Images in each experiment were batch-processed with uniform color-replacement settings using Photoshop Bridge. Image-based quantitative analysis of E-cadherin versus vimentin staining areas was performed with ImagePro-Plus, using the Count/Size tool. Two color masks were created using color cube analysis to separate labeled components based on spectral distribution. The count tool was then used to quantify relative percentages of E-cadherin versus vimentin staining areas. Masks were copied to black backgrounds to create the displayed images. Batch-processing ensured unbiased comparison of groups.

Clonogenicity, MTT assays

Clonogenicity was measured by seeding 6-well plates at 1,000 cells/well. After 7 days, colonies were stained with 0.5% crystal violet in 25% methanol and counted on high resolution digital images. Methylthiazonletetrazolium (MTT) assays were performed by seeding 3,000 cells/well (OCTT2) or 5,000 cells/well (SCC9) on 96-well plates, unless otherwise noted. Growth was quantified using a MTT Proliferation Kit (Invitrogen). Optical density in each well was measured at 590nm (OD-590nm), and values were normalized relative to OD-590nm for non-treated controls in drug treatment experiments.

Gene expression profiling

In three independent experiments, Ecad-hi and Ecad-lo subpopulations were sorted, and RNA was extracted using an RNAeasy Kit (Qiagen, Valencia, CA, USA) to generate triplicate samples. A TotalPrep RNA Amplification Kit (Ambion, Austin, TX, USA) generated biotinylated cRNA, which was hybridized and analyzed on Illumina HumanHT-12v3 Beadchips (Illumina, San Diego, CA, USA) per manufacturer protocols. Raw data underwent variance-stabilizing transformation and quantile normalization using the Bioconductor Lumi package (Du *et al.*, 2008). Probes below background level (detection *P* value <0.01) were excluded, and differential expression was identified with Bayes-adjusted variance analysis using the Bioconductor Limma package (Smyth, 2004). Gene identifications were made using false discovery rate adjusted *P* values of <0.05. Raw data is made available under Gene Expression Omnibus #18722.

Western blot analysis

Total cellular protein was extracted and blotted as described (Smalley *et al.*, 2005) using antibody to human EGFR (Santa Cruz). After analysis, western blots were stripped once and reprobed for β-actin to assess even protein loading.

Statistical methods

Data points with error bars show means ± standard error of mean (SEM) based on triplicate values. Differences are analyzed between individual data points by paired Student's *t*-test and between curves by ANOVA.

Supplementary Material

Refer to Web version on PubMed Central for supplementary material.

Acknowledgments

Grant support: NIH/NCI P01 CA098101 (M. Herlyn, A. Rustgi, and D. Basu) and ACS IRG-78-002-30 (D. Basu).

We acknowledge Fredrick Keeny in the Wistar Institute Microscopy Core for assistance with digital image processing and Ademi Santiago-Walker, PhD for critical review of the manuscript. This work is supported by grants from the NIH (NCI P01 CA098101) and the American Cancer Society (IRG-78-002-30). Work is also supported in part with resources and use of facilities at the Philadelphia VA Medical Center.

References

Adam L, Zhong M, Choi W, Qi W, Nicoloso M, Arora A, et al. miR-200 expression regulates epithelial-to-mesenchymal transition in bladder cancer cells and reverses resistance to epidermal growth factor receptor therapy. Clin Cancer Res. 2009; 15:5060–72. [PubMed: 19671845]

Ansieau S, Bastid J, Doreau A, Morel AP, Bouchet BP, Thomas C, et al. Induction of EMT by twist proteins as a collateral effect of tumor-promoting inactivation of premature senescence. Cancer Cell. 2008; 14:79–89. [PubMed: 18598946]

Bianco R, Troiani T, Tortora G, Ciardiello F. Intrinsic and acquired resistance to EGFR inhibitors in human cancer therapy. Endocr Relat Cancer. 2005; 12(Suppl 1):S159–71. [PubMed: 16113092]

Bonner JA, Harari PM, Giralt J, Azarnia N, Shin DM, Cohen RB, et al. Radiotherapy plus cetuximab for squamous-cell carcinoma of the head and neck. N Engl J Med. 2006; 354:567–78. [PubMed: 16467544]

Cano A, Perez-Moreno MA, Rodrigo I, Locascio A, Blanco MJ, del Barrio MG, et al. The transcription factor snail controls epithelial-mesenchymal transitions by repressing E-cadherin expression. Nat Cell Biol. 2000; 2:76–83. [PubMed: 10655586]

Christiansen JJ, Rajasekaran AK. Reassessing epithelial to mesenchymal transition as a prerequisite for carcinoma invasion and metastasis. Cancer Res. 2006; 66:8319–26. [PubMed: 16951136]

Chung CH, Ely K, McGavran L, Varella-Garcia M, Parker J, Parker N, et al. Increased epidermal growth factor receptor gene copy number is associated with poor prognosis in head and neck squamous cell carcinomas. J Clin Oncol. 2006; 24:4170–6. [PubMed: 16943533]

Cooper JB, Cohen EE. Mechanisms of resistance to EGFR inhibitors in head and neck cancer. Head Neck. 2009; 31:1086–94. [PubMed: 19378324]

Du P, Kibbe WA, Lin SM. lumi: a pipeline for processing Illumina microarray. Bioinformatics. 2008; 24:1547–8. [PubMed: 18467348]

Erjala K, Sundvall M, Junttila TT, Zhang N, Savisalo M, Mali P, et al. Signaling via ErbB2 and ErbB3 associates with resistance and epidermal growth factor receptor (EGFR) amplification with sensitivity to EGFR inhibitor gefitinib in head and neck squamous cell carcinoma cells. Clin Cancer Res. 2006; 12:4103–11. [PubMed: 16818711]

Fang D, Nguyen TK, Leishear K, Finko R, Kulp AN, Hotz S, et al. A tumorigenic subpopulation with stem cell properties in melanomas. Cancer Res. 2005; 65:9328–37. [PubMed: 16230395]

Frederick BA, Helfrich BA, Coldren CD, Zheng D, Chan D, Bunn PA Jr, et al. Epithelial to mesenchymal transition predicts gefitinib resistance in cell lines of head and neck squamous cell carcinoma and non-small cell lung carcinoma. Mol Cancer Ther. 2007; 6:1683–91. [PubMed: 17541031]

Fuchs BC, Fujii T, Dorfman JD, Goodwin JM, Zhu AX, Lanuti M, et al. Epithelial-to-mesenchymal transition and integrin-linked kinase mediate sensitivity to epidermal growth factor receptor inhibition in human hepatoma cells. Cancer Res. 2008; 68:2391–9. [PubMed: 18381447]

Gazdar AF. Activating and resistance mutations of EGFR in non-small-cell lung cancer: role in clinical response to EGFR tyrosine kinase inhibitors. Oncogene. 2009; 28(Suppl 1):S24–31. [PubMed: 19680293]

Ghoul A, Serova M, Astorgues-Xerri L, Bieche I, Bousquet G, Varna M, et al. Epithelial-to-mesenchymal transition and resistance to ingenol 3-angelate, a novel protein kinase C modulator, in colon cancer cells. Cancer Res. 2009; 69:4260–9. [PubMed: 19417139]

Gregory PA, Bert AG, Paterson EL, Barry SC, Tsykin A, Farshid G, et al. The miR-200 family and miR-205 regulate epithelial to mesenchymal transition by targeting ZEB1 and SIP1. Nat Cell Biol. 2008; 10:593–601. [PubMed: 18376396]

Haddad Y, Choi W, McConkey DJ. Delta-crystallin enhancer binding factor 1 controls the epithelial to mesenchymal transition phenotype and resistance to the epidermal growth factor receptor inhibitor erlotinib in human head and neck squamous cell carcinoma lines. Clin Cancer Res. 2009; 15:532–42. [PubMed: 19147758]

Herbst RS, Arquette M, Shin DM, Dicke K, Vokes EE, Azarnia N, et al. Phase II multicenter study of the epidermal growth factor receptor antibody cetuximab and cisplatin for recurrent and refractory squamous cell carcinoma of the head and neck. J Clin Oncol. 2005; 23:5578–87. [PubMed: 16009949]

Hugo H, Ackland ML, Blick T, Lawrence MG, Clements JA, Williams ED, et al. Epithelial--mesenchymal and mesenchymal--epithelial transitions in carcinoma progression. J Cell Physiol. 2007; 213:374–83. [PubMed: 17680632]

Kalyankrishna S, Grandis JR. Epidermal growth factor receptor biology in head and neck cancer. J Clin Oncol. 2006; 24:2666–72. [PubMed: 16763281]

Kawaguchi Y, Kono K, Mimura K, Mitsui F, Sugai H, Akaike H, et al. Targeting EGFR and HER-2 with cetuximab- and trastuzumab-mediated immunotherapy in oesophageal squamous cell carcinoma. Br J Cancer. 2007; 97:494–501. [PubMed: 17622245]

Kurrey NK, Jalgaonkar SP, Joglekar AV, Ghanate AD, Chaskar PD, Doiphode RY, et al. Snail and slug mediate radioresistance and chemoresistance by antagonizing p53-mediated apoptosis and acquiring a stem-like phenotype in ovarian cancer cells. Stem Cells. 2009; 27:2059–68. [PubMed: 19544473]

Li C, Iida M, Dunn EF, Ghia AJ, Wheeler DL. Nuclear EGFR contributes to acquired resistance to cetuximab. Oncogene. 2009a

Li QQ, Xu JD, Wang WJ, Cao XX, Chen Q, Tang F, et al. Twist1-mediated adriamycin-induced epithelial-mesenchymal transition relates to multidrug resistance and invasive potential in breast cancer cells. Clin Cancer Res. 2009b; 15:2657–65. [PubMed: 19336515]

Li Y, VandenBoom TG 2nd, Kong D, Wang Z, Ali S, Philip PA, et al. Up-regulation of miR-200 and let-7 by natural agents leads to the reversal of epithelial-to-mesenchymal transition in gemcitabine-resistant pancreatic cancer cells. Cancer Res. 2009c; 69:6704–12. [PubMed: 19654291]

Mancaniello D, Carbonari M. Immunophenotyping and DNA content analysis of acetone-fixed cells. Curr Protoc Cytom. 2008; Chapter 9(Unit 9):26. [PubMed: 18972368]

Mandal M, Myers JN, Lippman SM, Johnson FM, Williams MD, Rayala S, et al. Epithelial to mesenchymal transition in head and neck squamous carcinoma: association of Src activation with E-cadherin down-regulation, vimentin expression, and aggressive tumor features. Cancer. 2008; 112:2088–100. [PubMed: 18327819]

Mani SA, Guo W, Liao MJ, Eaton EN, Ayyanan A, Zhou AY, et al. The epithelial-mesenchymal transition generates cells with properties of stem cells. Cell. 2008; 133:704–15. [PubMed: 18485877]

Okano J, Gaslightwala I, Birnbaum MJ, Rustgi AK, Nakagawa H. Akt/protein kinase B isoforms are differentially regulated by epidermal growth factor stimulation. J Biol Chem. 2000; 275:30934–42. [PubMed: 10908564]

Opitz OG, Jenkins TD, Rustgi AK. Transcriptional regulation of the differentiation-linked human K4 promoter is dependent upon esophageal-specific nuclear factors. J Biol Chem. 1998; 273:23912–21. [PubMed: 9727005]

Peinado H, Olmeda D, Cano A. Snail, Zeb and bHLH factors in tumour progression: an alliance against the epithelial phenotype? Nat Rev Cancer. 2007; 7:415–28. [PubMed: 17508028]

Posner MR, Hershock DM, Blajman CR, Mickiewicz E, Winquist E, Gorbounova V, et al. Cisplatin and fluorouracil alone or with docetaxel in head and neck cancer. N Engl J Med. 2007; 357:1705–15. [PubMed: 17960013]

Rheinwald JG, Beckett MA. Tumorigenic keratinocyte lines requiring anchorage and fibroblast support cultures from human squamous cell carcinomas. Cancer Res. 1981; 41:1657–63. [PubMed: 7214336]

Shackleton M, Quintana E, Fearon ER, Morrison SJ. Heterogeneity in cancer: cancer stem cells versus clonal evolution. Cell. 2009; 138:822–9. [PubMed: 19737509]

Shrader M, Pino MS, Brown G, Black P, Adam L, Bar-Eli M, et al. Molecular correlates of gefitinib responsiveness in human bladder cancer cells. Mol Cancer Ther. 2007; 6:277–85. [PubMed: 17237287]

Smalley KS, Brafford P, Haass NK, Brandner JM, Brown E, Herlyn M. Up-regulated expression of zonula occludens protein-1 in human melanoma associates with N-cadherin and contributes to invasion and adhesion. Am J Pathol. 2005; 166:1541–54. [PubMed: 15855653]

Smalley KS, Haass NK, Brafford PA, Lioni M, Flaherty KT, Herlyn M. Multiple signaling pathways must be targeted to overcome drug resistance in cell lines derived from melanoma metastases. Mol Cancer Ther. 2006; 5:1136–44. [PubMed: 16731745]

Smyth GK. Linear models and empirical bayes methods for assessing differential expression in microarray experiments. Stat Appl Genet Mol Biol. 2004; 3 Article3.

Strauss R, Sova P, Liu Y, Li ZY, Tuve S, Pritchard D, et al. Epithelial phenotype confers resistance of ovarian cancer cells to oncolytic adenoviruses. Cancer Res. 2009; 69:5115–25. [PubMed: 19491256]

Tarin D, Thompson EW, Newgreen DF. The fallacy of epithelial mesenchymal transition in neoplasia. Cancer Res. 2005; 65:5996–6000. discussion 6000–1. [PubMed: 16024596]

Temam S, Kawaguchi H, El-Naggar AK, Jelinek J, Tang H, Liu DD, et al. Epidermal growth factor receptor copy number alterations correlate with poor clinical outcome in patients with head and neck squamous cancer. J Clin Oncol. 2007; 25:2164–70. [PubMed: 17538160]

Thomson S, Buck E, Petti F, Griffin G, Brown E, Ramnarine N, et al. Epithelial to mesenchymal transition is a determinant of sensitivity of non-small-cell lung carcinoma cell lines and xenografts

to epidermal growth factor receptor inhibition. Cancer Res. 2005; 65:9455–62. [PubMed: 16230409]

Vermorken JB, Remenar E, van Herpen C, Gorlia T, Mesia R, Degardin M, et al. Cisplatin, fluorouracil, and docetaxel in unresectable head and neck cancer. N Engl J Med. 2007; 357:1695–704. [PubMed: 17960012]

Wang Z, Li Y, Kong D, Banerjee S, Ahmad A, Azmi AS, et al. Acquisition of epithelial-mesenchymal transition phenotype of gemcitabine-resistant pancreatic cancer cells is linked with activation of the notch signaling pathway. Cancer Res. 2009; 69:2400–7. [PubMed: 19276344]

Wu K, Bonavida B. The activated NF-kappaB-Snail-RKIP circuitry in cancer regulates both the metastatic cascade and resistance to apoptosis by cytotoxic drugs. Crit Rev Immunol. 2009; 29:241–54. [PubMed: 19538137]

Yang AD, Fan F, Camp ER, van Buren G, Liu W, Somcio R, et al. Chronic oxaliplatin resistance induces epithelial-to-mesenchymal transition in colorectal cancer cell lines. Clin Cancer Res. 2006; 12:4147–53. [PubMed: 16857785]

Yauch RL, Januario T, Eberhard DA, Cavet G, Zhu W, Fu L, et al. Epithelial versus mesenchymal phenotype determines in vitro sensitivity and predicts clinical activity of erlotinib in lung cancer patients. Clin Cancer Res. 2005; 11:8686–98. [PubMed: 16361555]

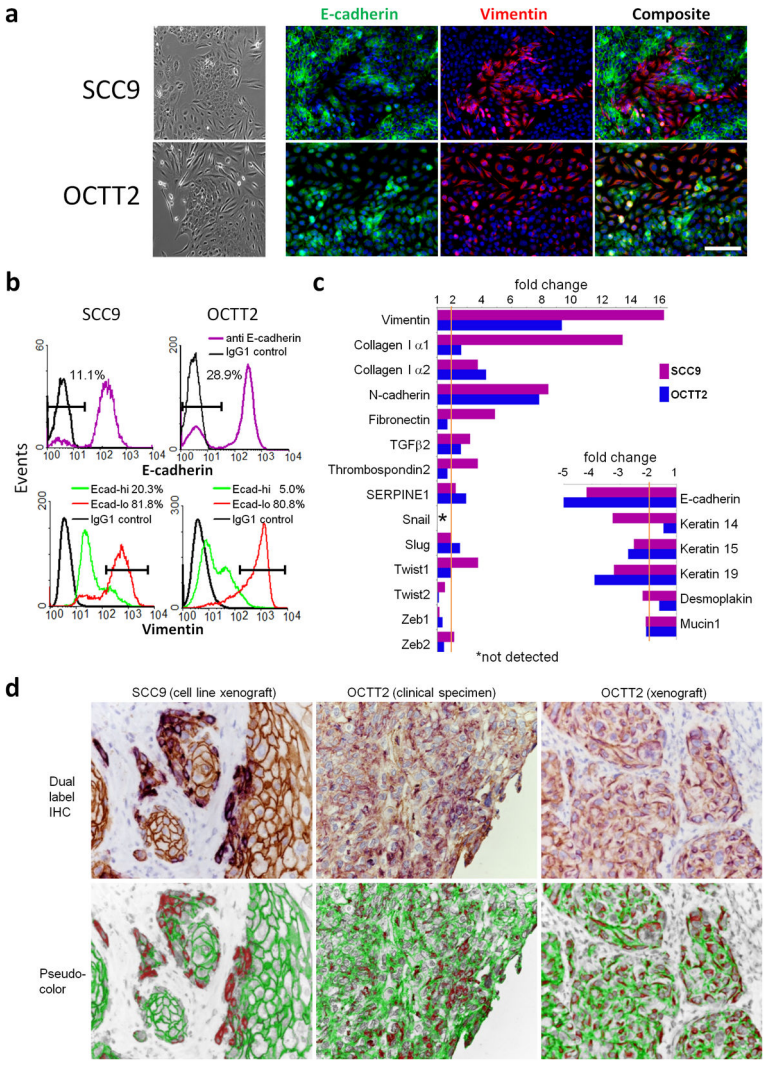

Figure 1. Distinct epithelial and mesenchymal-like subpopulations *in vitro* and *in vivo*

(a) Phase contrast (10x) of heterogeneity in SCC9 and OCTT2 lines (left panels); IF (20x) of SCC9 and OCTT2 lines stained for 4′,6-diamidino-2-phenylindole (DAPI, blue), E-cadherin (green), and vimentin (red) (right panels). Fields were selected to contain both subpopulations in equal proportion. Bar=100μm. **(b)** SCC9 and OCTT2 cell lines segregated by FACS into Ecad-hi and Ecad-lo subsets (top panels); sorted subsets were then permeabilized and compared for vimentin staining using FC (bottom panels). **(c)** Gene expression profiling compares Ecad-hi vs. Ecad-lo subpopulations in SCC9 and OCTT2 lines. Expression of genes up-regulated (left panel) or down-regulated (right panel) during EMT is displayed as fold-change in Ecad-lo relative to Ecad-hi cells. **(d)** Dual label IHC for E-cadherin (brown) and vimentin (purple) in xenografts of SCC9 cells (left), the clinical HNSCC specimen from which the OCTT2 line was derived (middle), and xenografts of that clinical specimen (right) (40x, top row); corresponding digital pseudo-color images (bottom row), in which E-cadherin is green and vimentin is red. SCC9 xenografts were grown for 5–6 weeks after subcutaneous injection. OCTT2 xenografts were grown for 3 weeks post-

implantation. Sections are representative of at least 4 mice analyzed per group. Data in (a) and (b) represent at least 3 independent experiments.

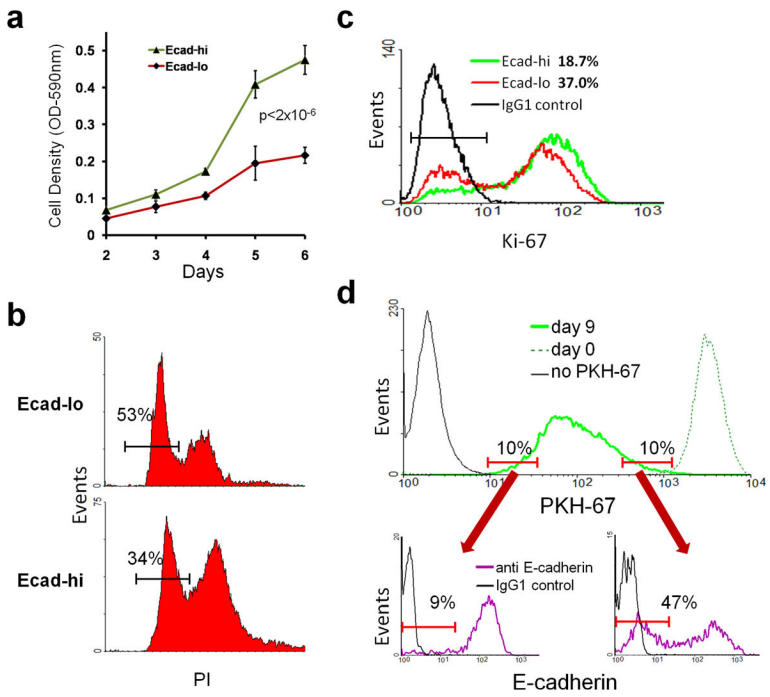

Figure 2. Reduced proliferation in the mesenchymal-like subset

(a) SCC9 cells were sorted into Ecad-hi and Ecad-lo subpopulations, and growth of each was measured by MTT assay. **(b)** Percentage of each subpopulation in G0/G1 phase, quantified by PI staining. **(c)** Percentage of each subpopulation in G0 phase, compared using FC of Ki-67 staining. **(d)** SCC9 cells were labeled with PKH-67, and uniform labeling was confirmed by FC at day 0 (top panel, dashed line). After growth for 9 days, cells were reanalyzed to determine the distribution of PKH-67 fluorescence (solid green line). The size of the Ecad-lo subset was compared between the 10% of cells with lowest PKH-67 label retention (left lower panel) versus the 10% of cells with highest label retention (right lower panel). Data are representative of 3 independent experiments.

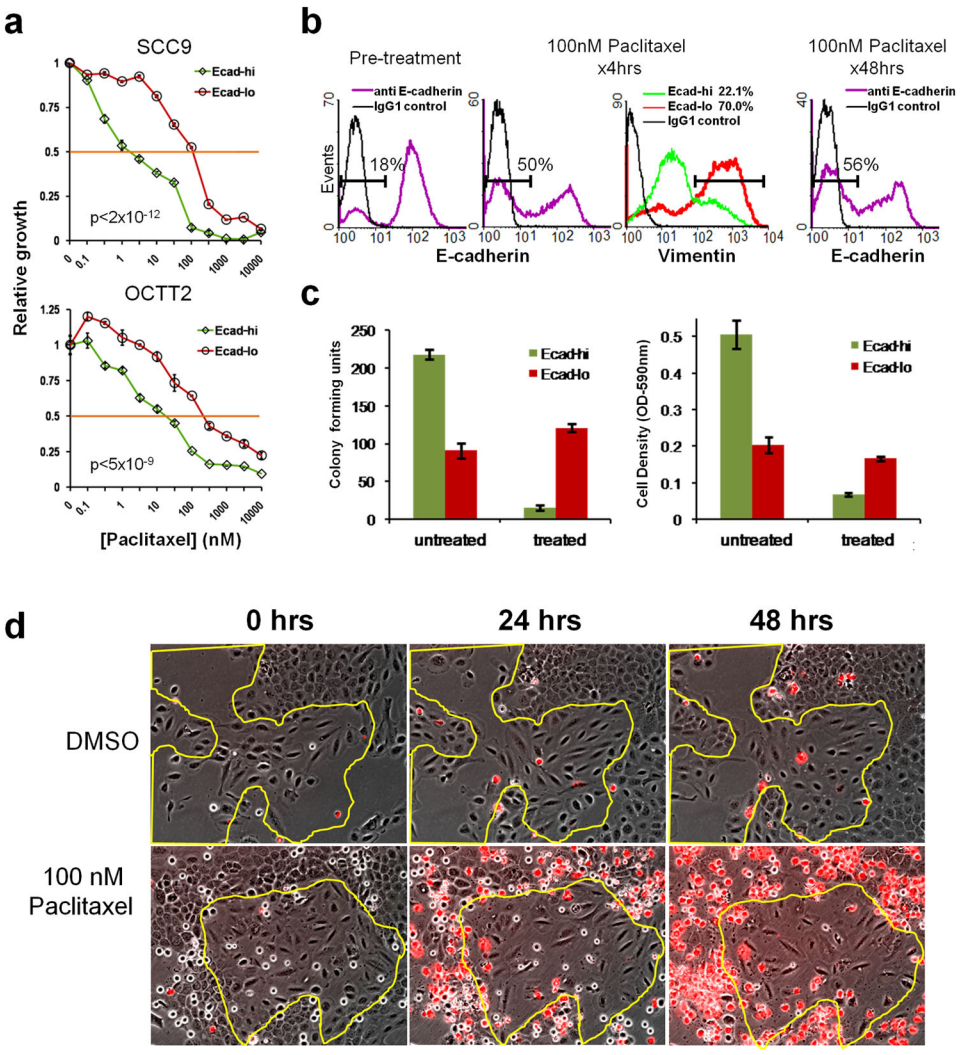

Figure 3. Intrinsic paclitaxel resistance in the mesenchymal-like subset

(a) Ecad-hi and Ecad-lo subpopulations of SCC9/OCTT2 cells were treated with paclitaxel for 4 hours. Drug-induced growth inhibition is shown 72 hours later by MTT assay. **(b)** SCC9 cells were exposed to 100nM paclitaxel for 4 hrs. After 72 hours, the percentage of Ecad-lo cells among total viable cells pre vs. post-drug treatment is compared by FC (left and second panel). Cells surviving paclitaxel were sorted into Ecad-hi and Ecad-lo subsets and analyzed for vimentin expression (third panel). The percentage of Ecad-lo cells present after 48 continuous hours of paclitaxel exposure was also measured (right panel). **(c)** The same subsets treated with paclitaxel for 4 hours were compared against untreated controls for clonogenicity (left) and total growth after 72 hours (right) by MTT. **(d)** SCC9 cells treated with 100nM paclitaxel or DMSO control for 4 hours were observed by video microscopy in the presence of PI. Representative still images at 0, 24, and 48 hours (20x) after treatment identify cell death with PI uptake (red). Yellow lines encompass areas of mesenenchymal-like morphology. Data in (a)–(c) are representative of 3 independent experiments.

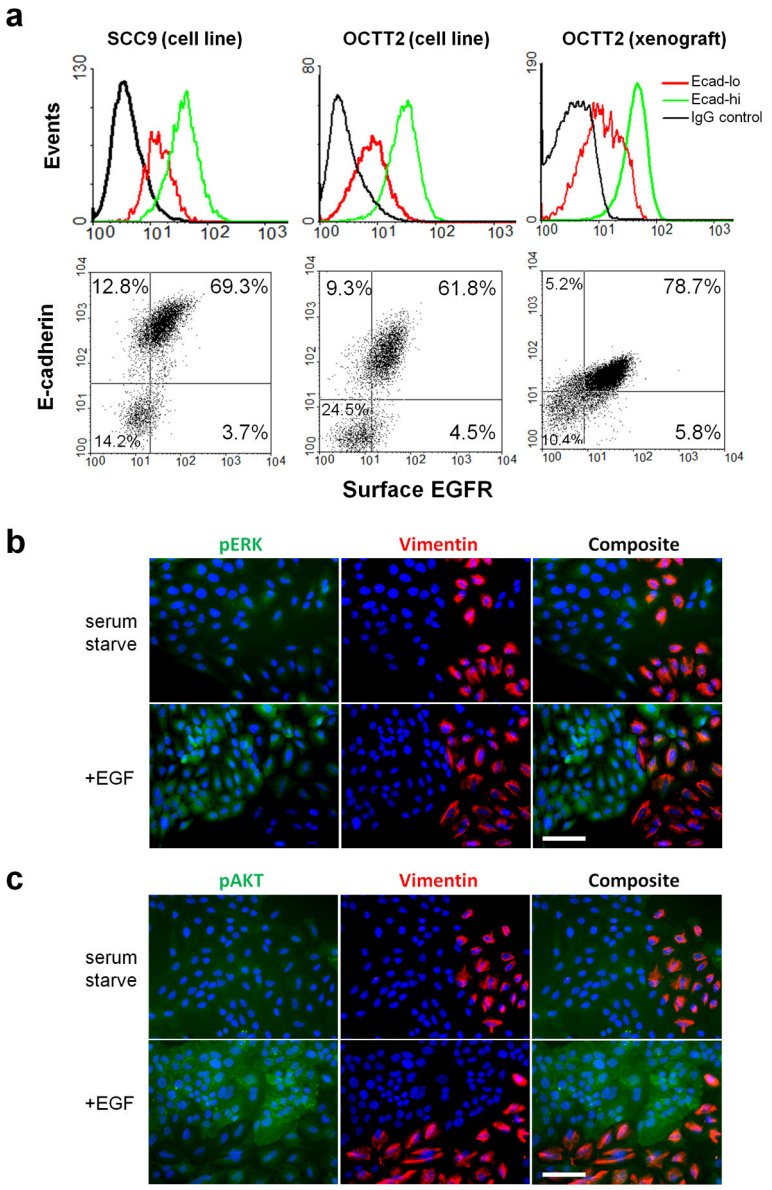

Figure 4. Diminished EGFR expression and regulation of MAPK/PI3K pathways in the mesenchymal like subset

(a) Ecad-hi vs. Ecad-lo SSC9 cells (left panels) and OCTT2 cells (middle panels) were analyzed by FC for surface EGFR expression. Surface EGFR levels are compared between subpopulations in tumor cells purified from xenografts of the OCTT2 clinical specimen (right panels). **(b,c)** IF (20x) of serum-starved SCC9 cells, with or without added 200ng/ml EGF, stained for DAPI (blue), vimentin (red), and either pERK (green, panel C) or pAKT (green, panel D). Results are representative of 3 independent experiments. Bars=100μm.

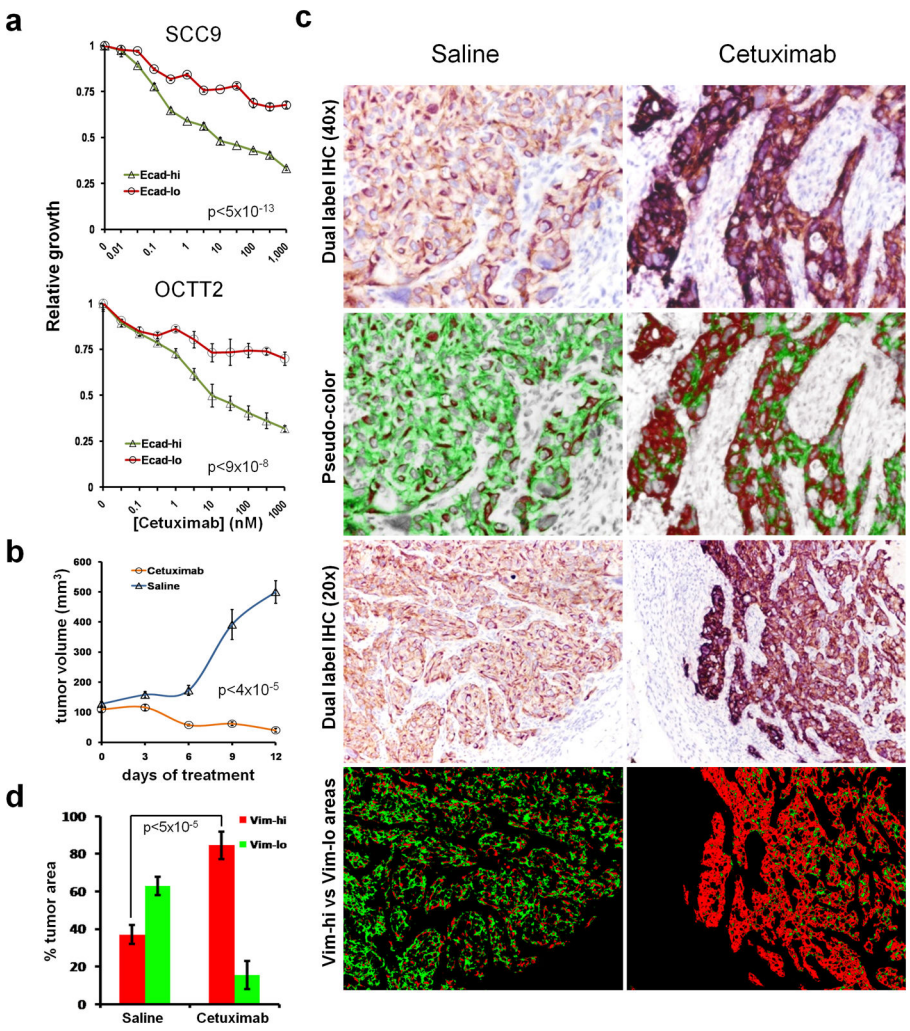

Figure 5. Intrinsic resistance to cetuximab in the mesenchymal-like subpopulation

(a) Growth inhibition of Ecad-hi and Ecad-lo subpopulations in SCC9 and OCTT2, measured by MTT assay after 72 hours cetuximab treatment. Data represent 3 independent experiments. **(b)** Xenografts were established of the human tumor from which the OCTT2 line originated, and mice with 100mm^3 tumors were treated with 1mg cetuximab every 3 days for 4 doses. Tumor volume is plotted in comparison to saline-injected controls (n=4/group). **(c)** Cetuximab-treated and control tumors harvested after 12 days treatment were stained using dual label IHC (first row, 40x) for E-cadherin (brown) and vimentin (purple). Pseudo-color images (second row) show E-cadherin in green and vimentin in red. Vim-hi and vim-lo zones in wide areas of dual IHC-stained tumors (third row, 20x) were mapped in red and green, respectively, with exclusion of stromal areas and nuclei from analysis (fourth row). **(d)** Relative percentages of vim-hi versus vim-lo areas quantified in treated versus untreated tumors (n=4/group).

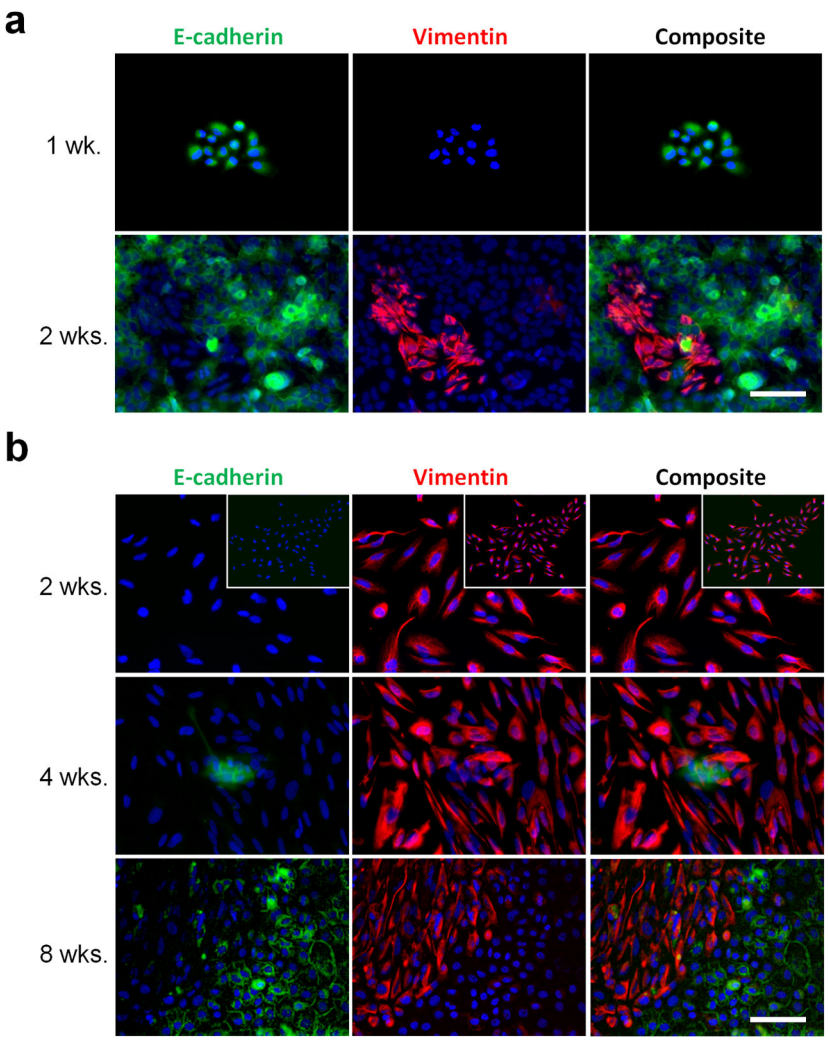

Figure 6. Dynamic reversibility of epithelial and mesenchymal-like phenotypes at a clonal level

(a) Ecad-hi SCC9 cells were plated at clonal dilution, and wells containing single colonies with pure epithelial morphology are identified after 1 week (top, 20x) by staining for DAPI (blue), E-cadherin (green), and vimentin (red). Similar morphologically pure colonies were expanded and then stained at 2 weeks (bottom). **(b)** Ecad-lo SCC9 cells were plated at clonal dilution, and wells containing isolated colonies with pure mesenchymal-like morphology are identified at 2 weeks and stained as in (a) (top row; 20x, inset 10x). Comparable colonies were expanded until epithelial areas initially appeared at 4 weeks (middle row) or fully repopulated after 8 weeks (bottom row). Bars=100μm.